The Astronomical Journal, 127:3609–3621, 2004 June

VLBI OBSERVATIONS OF SOUTHERN HEMISPHERE ICRF SOURCES. I.

Roopesh Ojha,[1] Alan L. Fey,[2] Kenneth J. Johnston,[2] David L. Jauncey,[1] John E. Reynolds,[1] Anastasios K. Tzioumis,[1] Jonathan F. H. Quick,[3] George D. Nicolson,[3] Simon P. Ellingsen,[4] Richard G. Dodson,[4] and Peter M. McCulloch[4]

Received 2004 February 6; accepted 2004 March 9

ABSTRACT

We present 8.4 GHz very long baseline interferometry (VLBI) observations of 69 southern hemisphere extragalactic sources in the International Celestial Reference Frame. These are the first in a series of observations intended to image all such sources at milliarcsecond resolution in order to determine their continued suitability for reference-frame use based on intrinsic structure. We use the resultant images to calculate a core fraction, that is, the ratio of core flux density to total flux density, for all observed sources. The resulting distribution, with a mean value of 0.83, suggests that most sources are relatively compact. However, just over half the observed sources show significant extended emission in the form of multiple compact components. These sources are probably poorly suited for high-accuracy reference-frame use unless intrinsic structure and potential variability can be taken into account. Our observations represent the first large, comprehensive VLBI imaging survey in the southern hemisphere, significantly extending the existing limited VLBI surveys and, along with some well-known objects, containing many sources that have never been imaged at milliarcsecond resolution. The overlap with Very Long Baseline Array images of sources between 0° and −35° declination helps determine the limits to imaging with the southern hemisphere–accessible telescopes.

Key words: astrometry — galaxies: active — quasars: general — radio continuum: galaxies — reference systems — surveys

On-line material: machine-readable tables

1. INTRODUCTION

Since the late 1970s, very long baseline interferometry (VLBI) observations at two frequencies, 8.4 (X band) and 2.3 GHz (S band), have been used to determine the positions of compact radio sources with unprecedented accuracy. The basic observable is the group delay, with the use of two frequencies allowing calibration of the frequency-dependent propagation delay in the ionosphere. Observations of selected strong compact extragalactic radio sources, using this now mature technique, have been used to define and maintain a radio reference frame with sub-milliarcsecond precision. Johnston et al. (1988) set out to establish a global reference frame of 400 sources in 1986. The first catalog produced (Ma et al. 1990) had 182 sources with a positional accuracy of 1 milliarcsecond (mas), all located north of −30°. Subsequent observing campaigns increased the density of sources in the northern hemisphere and added sources in the southern hemisphere (Russell et al. 1994; Reynolds et al. 1994; Johnston et al. 1995). The current realization of the celestial frame is the International Celestial Reference Frame (ICRF; Ma et al. 1998), which was adopted by the 23rd IAU General Assembly in 1997 to replace the traditional optical fundamental reference system, the FK5 reference frame, as the fundamental celestial reference frame. The ICRF replaced the FK5 stellar catalog as the fundamental celestial reference frame as of 1998 January 1 and is the realization of the International Celestial Reference System (ICRS) at radio wavelengths, with a precision of approximately 20 microarcseconds per coordinate axis. The *Hipparcos* Catalogue (Perryman et al. 1997) is the realization of the ICRS at optical wavelengths (Kovalevsky et al. 1997).

Extragalactic radio sources, such as those that define the ICRF, display a variety of structure down to milliarcsecond scales. Further, they exhibit flux density variability on timescales of years to weeks and also display structural variability at milliarcsecond scales. This departure from the point-source approximation commonly made in astrometric analysis introduces error in the observable quantities (group delay and delay rate). The effect of source structure on VLBI astrometric positions can be significant (see, e.g., Charlot 1990; Fey & Charlot 1997). Also, as the structure of these sources varies with time, it is important to image their structure at several epochs in order to define a time-dependent source model. Multiepoch observations, using the Very Long Baseline Array (VLBA), to image northern hemisphere sources at 8.4 GHz have been progressing successfully (Fey & Charlot 2000).

We have used the Australian Long Baseline Array, augmented by telescopes in South Africa and Hawaii, to image 69 ICRF sources at 8.4 GHz. These are the first results from a multiepoch observing program that seeks to image, a minimum of two times, all existing southern hemisphere ICRF sources, as well as new additions being made as part of this program. These images will allow the evaluation of the continued suitability of these sources for reference-frame use based on their intrinsic source structure and structural variability.

In addition to the imaging observations, we have been making short survey observations of potential new astrometry sources. It is well known that there is a deficit of ICRF sources in the southern hemisphere (Ma et al. 1998). For example, of the 212 ICRF defining sources, less than 30% are in the southern hemisphere. In order to control local deformations of the ICRF,

[1] Australia Telescope National Facility, CSIRO, P.O. Box 76, Epping, NSW 1710, Australia.
[2] US Naval Observatory, 3450 Massachusetts Avenue, NW, Washington, DC 20392-5420.
[3] Hartebeesthoek Radio Astronomy Observatory, P.O. Box 443, Krugersdorp 1740, South Africa.
[4] School of Mathematics and Physics, University of Tasmania, Private Bag 37, Hobart, Tasmania 7001, Australia.

TABLE 1
THE LONG BASELINE ARRAY

Telescope	Diameter (m)	SEFD[a] (Jy)	Location
Parkes	64	90	Parkes, New South Wales
ATCA	5×22	80	Narrabri, New South Wales
Mopra	22	400	Coonabarabran, New South Wales
Hobart	26	750	Mount Pleasant, Tasmania
Ceduna	30	600	Ceduna, South Australia
Hartebeesthoek[b]	26	560	Hartebeesthoek, South Africa
Kokee[b]	20	900	Kokee Park, Hawaii

[a] System equivalent flux density.
[b] Affiliated telescopes.

it is crucial to increase the density of sources in the southern hemisphere. Despite the fact that 109 new sources were added to the ICRF in the ICRF-Ext.2 (Fey et al. 2004a), only four of these new sources were south of declination -30°. Based on our imaging observations, astrometric observations of candidate ICRF sources are in progress. Initial results for 22 sources are reported in Fey et al. (2004b).

As the first comprehensive survey of extragalactic sources in the southern hemisphere, our imaging program greatly extends existing, limited surveys (Preston et al. 1989; Shen et al. 1997, 1998). In addition to yielding source structure information for astrometric purposes, in most cases these are the first VLBI images of these flat-spectrum, extragalactic sources. Past experience, for example, the Pearson-Readhead survey and follow-up surveys (Taylor et al. 1996; Pearson & Readhead 1988), shows that such extensive surveys are a powerful tool not only for astrometry, but also for investigation of a wide range of astrophysical phenomena (e.g., Ojha et al. 2004).

2. OBSERVATIONS

The observations reported in this paper were made using the five telescopes that make up the Australian Long Baseline Array (LBA),[5] as well as telescopes in South Africa and Hawaii. Details of these telescopes are summarized in Table 1.

Because of limited mutual visibility between the last two sites, each observing epoch is split into two sessions, one involving observation with the LBA and South Africa and the other involving observation with the LBA and Hawaii. The data from the two epochs are calibrated separately and then combined in order to image with the best possible *u-v* plane coverage. Images from two epochs are presented here. The first epoch consisted of a 24 hr session with the LBA and Kokee on 2002 July 16, followed by a 48 hr session with the LBA and Hartebeesthoek from 2002 July 18 through July 20. The second epoch consisted of a 24 hr session with the LBA and Hartebeesthoek on 2002 November 14, followed by a 48 hr session with the LBA and Kokee on 2002 November 15 and 16.

At our observing frequency of 8.4 GHz, the LBA in these configurations yielded a *typical* angular resolution (synthesized beam) 1.5 by 0.7 mas in size, with the highest resolution in the east-west direction. Each source was observed in 10 to 12 scans of approximately 9 minutes each. After accounting for slew time, the *typical* on-source time was about 60 to 70 minutes.

[5] The Long Baseline Array is part of the Australia Telescope, which is funded by the Commonwealth of Australia for operation as a National Facility managed by CSIRO.

The data were recorded in S2 format (Cannon et al. 1997) and correlated at the Australia Telescope National Facility (ATNF) correlator located in Epping, New South Wales (Wilson, Roberts, & Davis 1996). These data have only one intermediate frequency, with a bandwidth of 8 MHz per polarization. The correlated data were processed using the National Radio Astronomy Observatory's Astronomical Image Processing System (AIPS) software (Bridle & Greisen 1994; Greisen 1988). The data were loaded using the locally written AIPS task ATLOD, which is needed to read the data in the format that the LBA generates. Thereafter, data inspection, initial editing, and fringe fitting were done in the standard manner using AIPS.

Overall amplitude calibration was improved using observations of known sources with $\geq$90% of their correlated flux in a compact core (Fey, Clegg, & Fomalont 1996). A single amplitude gain correction factor was derived for each antenna based on fitting a simple Gaussian source model to the visibility data of the respective compact source after applying only the initial calibration based on the measured system temperatures and gain curves. Gain correction factors were calculated based on the differences between the observed and model visibilities. The resulting set of amplitude gain correction factors was then applied to the visibility data of the target sources. Finally, the visibility data were Fourier inverted and CLEANed using the Caltech Difmap package (Shepherd 1997). The data were self-calibrated following the hybrid imaging technique of Pearson & Readhead (1984) to correct for residual amplitude and phase errors.

3. RESULTS

Contour plots of the final, naturally weighted images of 69 sources are shown in Figure 1. Five of these 69 sources, PKS 0332−403, PKS 1519−273, PKS 1622−297, PKS 1908−201, and PKS 1934−638, have been observed at two epochs and both images are shown. Table 2 lists parameters of all the images. Following the source name, the next three columns list the major axis, minor axis, and position angle of the beam. The next two columns list the peak and rms flux densities of the image. The final column indicates the contour levels used for each image. Physical characteristics of all sources (where available) are summarized in Table 3, which lists their optical identification and redshift, as well as visual magnitude.

The average rms noise in the images is $\sim$1.7 mJy beam^{-1} with a median rms of $\sim$0.8 mJy beam^{-1}. The distribution of image dynamic range (defined as image peak flux density divided by image rms) is shown in Figure 2. Values range from a high of 3600 (this outlier is not shown in Fig. 2) to a low of 50 (with one outlier with a value of 10). The mean value is 595

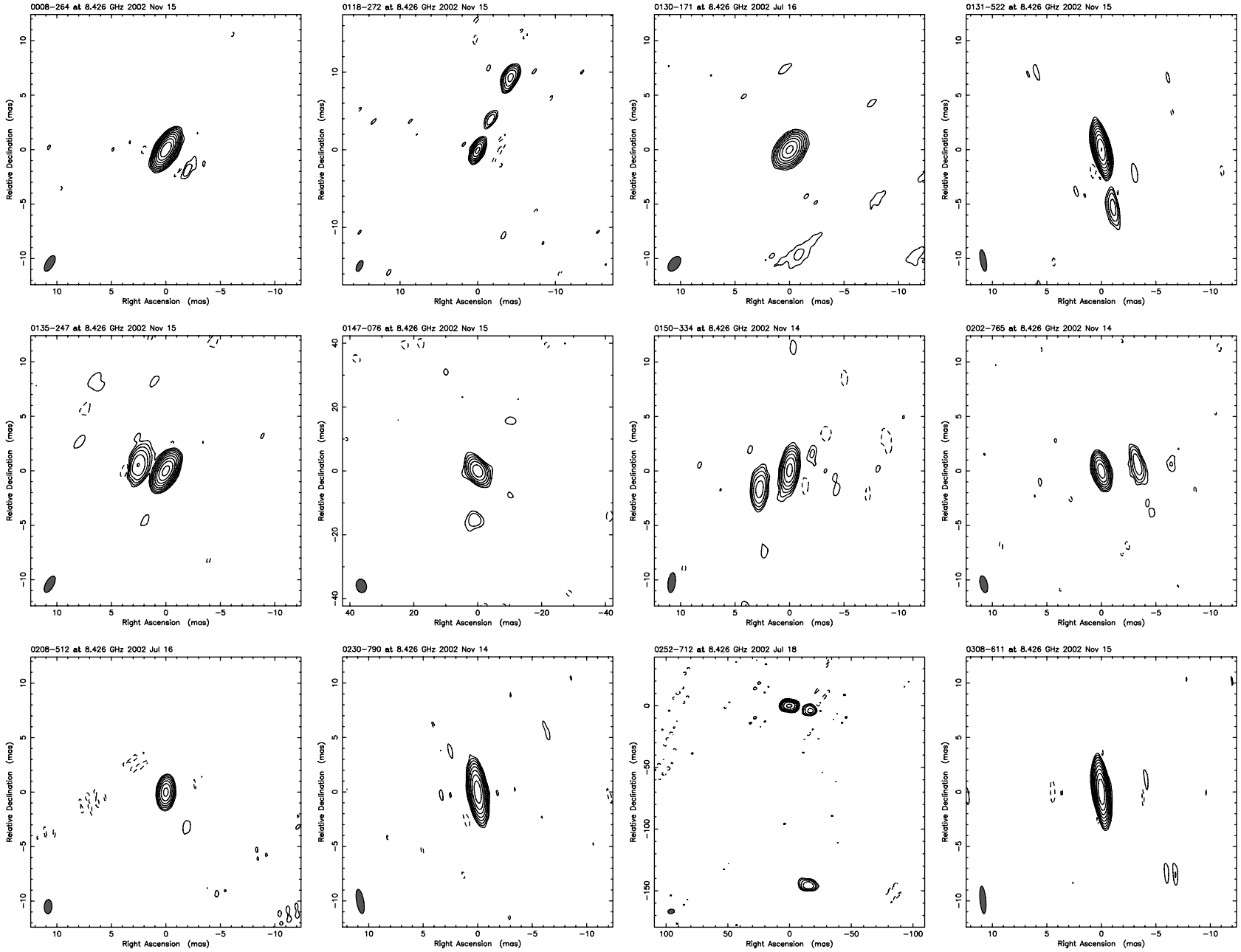

FIG. 1.—Contour plots of 69 extragalactic radio sources at 8.4 GHz. Image parameters are listed in Table 2. Gaussian models fitted to the visibility data are listed in Table 4. The scale of each image is in milliarcseconds. The FWHM Gaussian restoring beam applied to the images is shown as a hatched ellipse in the lower left of each panel.

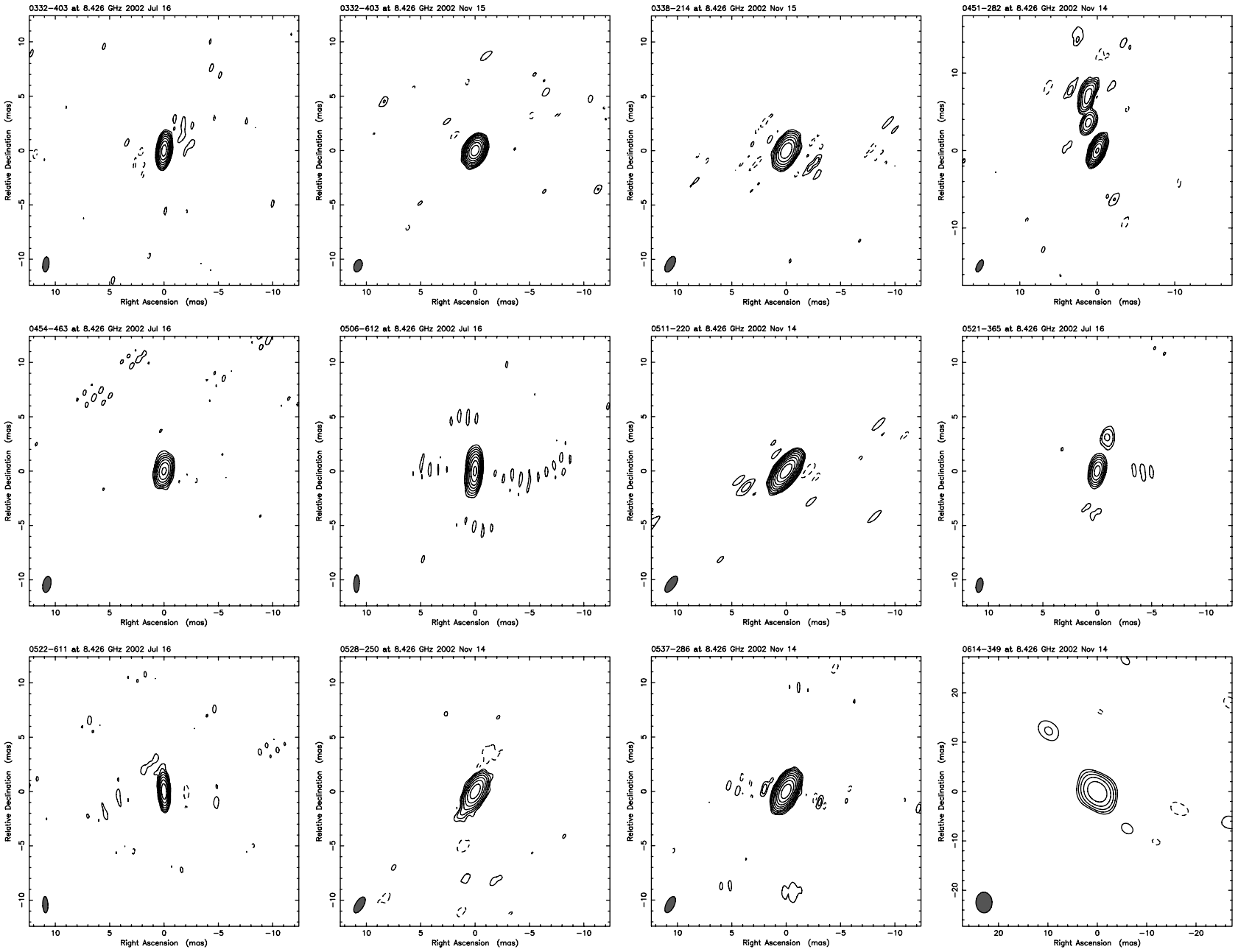

FIG. 1.—*Continued*

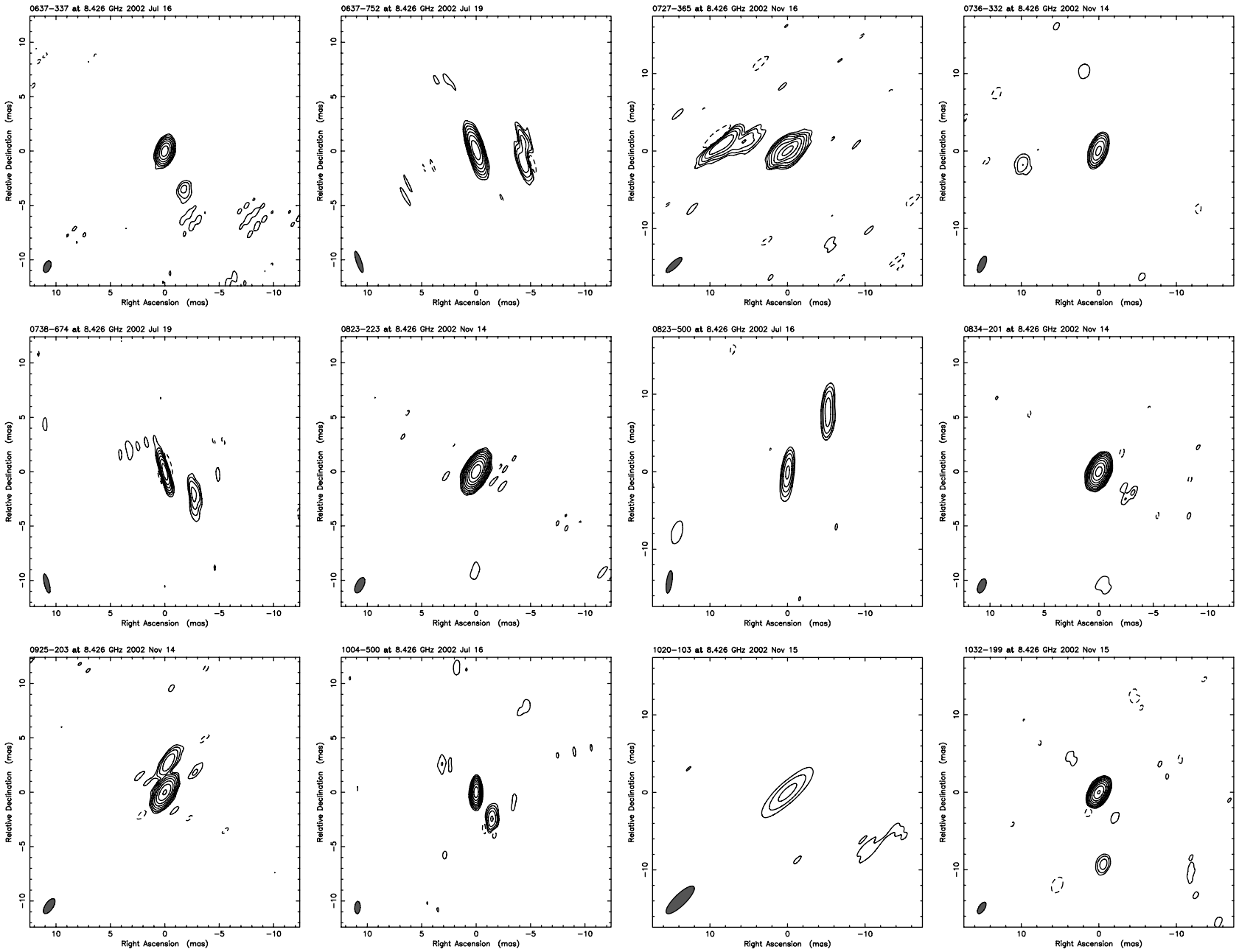

FIG. 1.—*Continued*

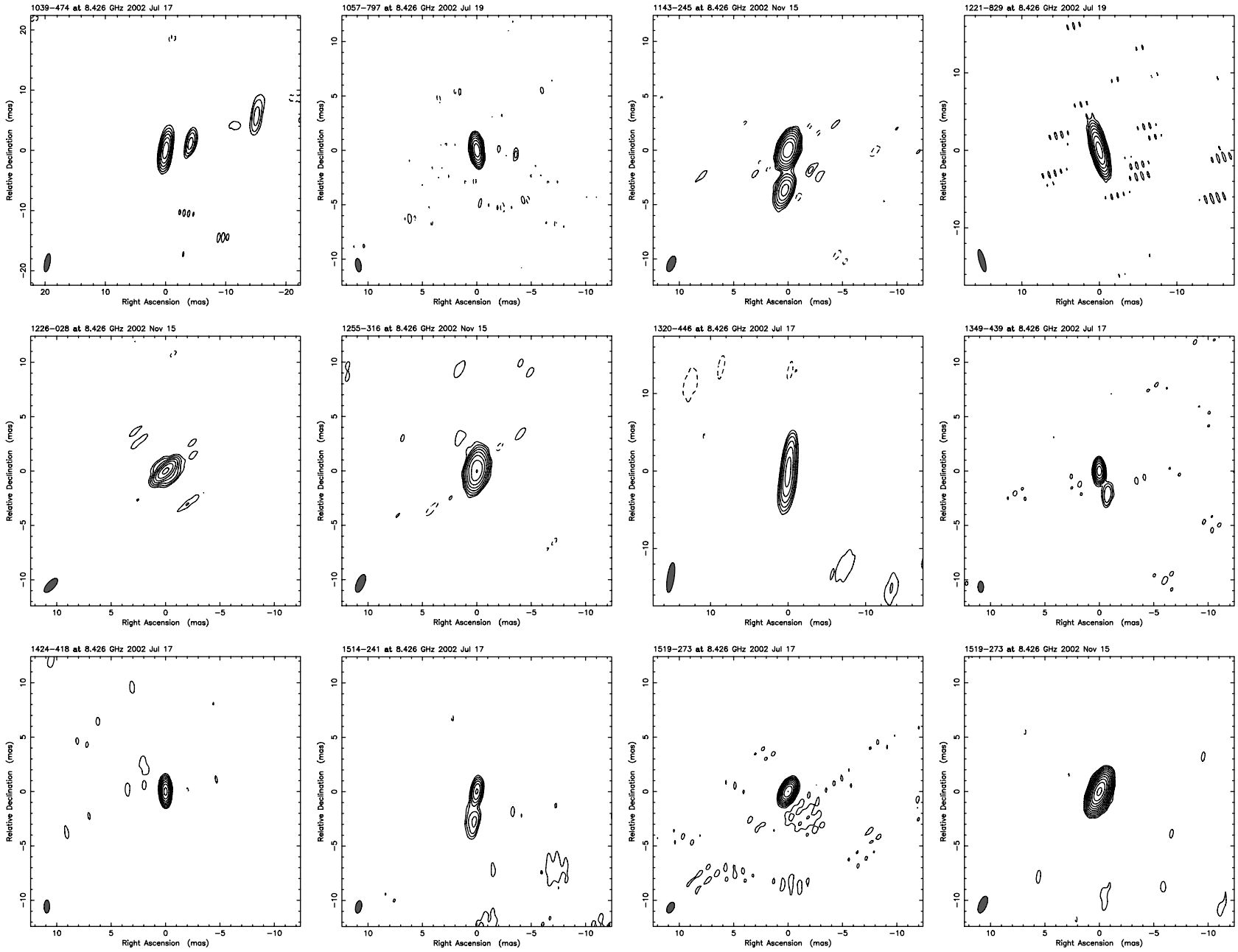

FIG. 1.—*Continued*

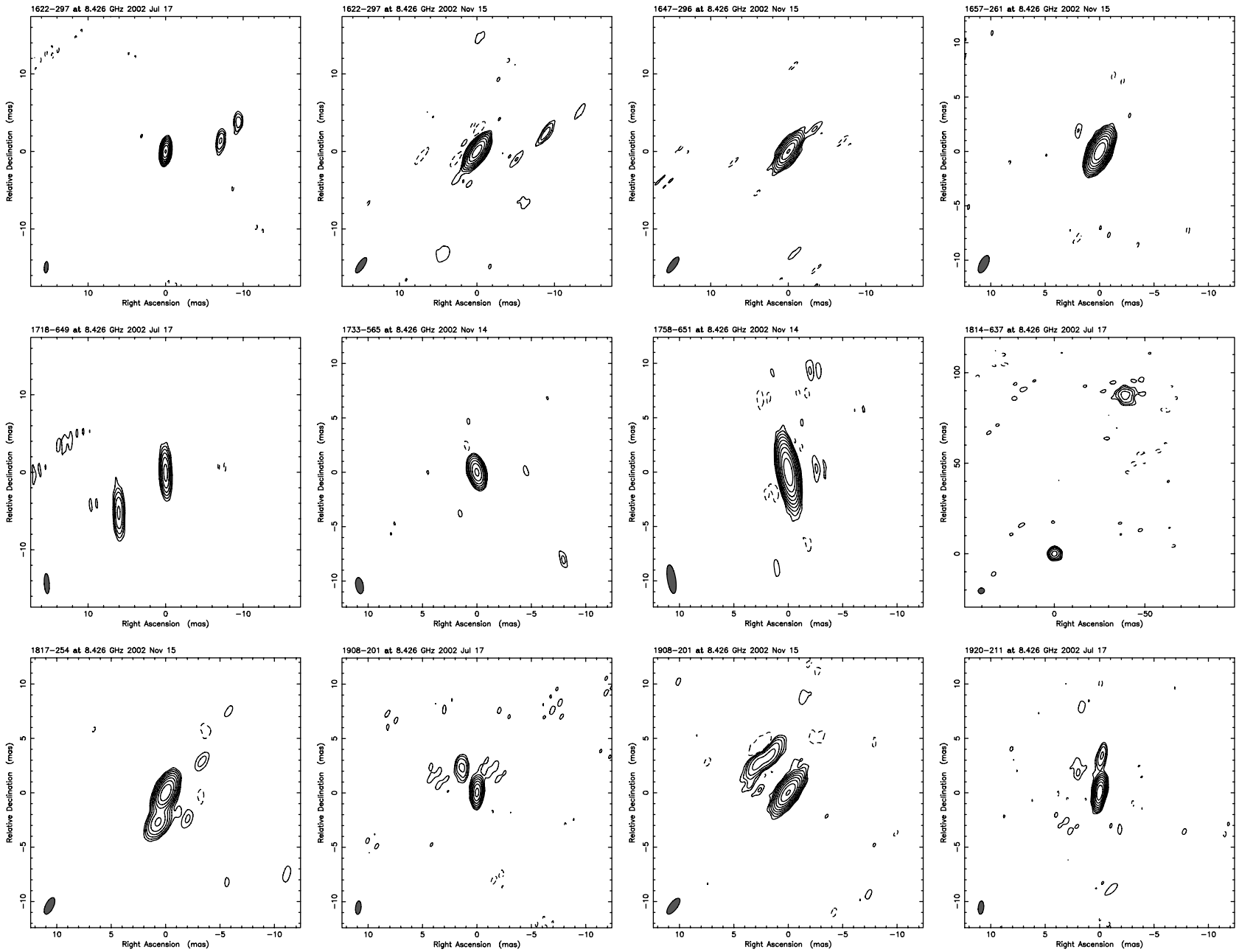

FIG. 1.—*Continued*

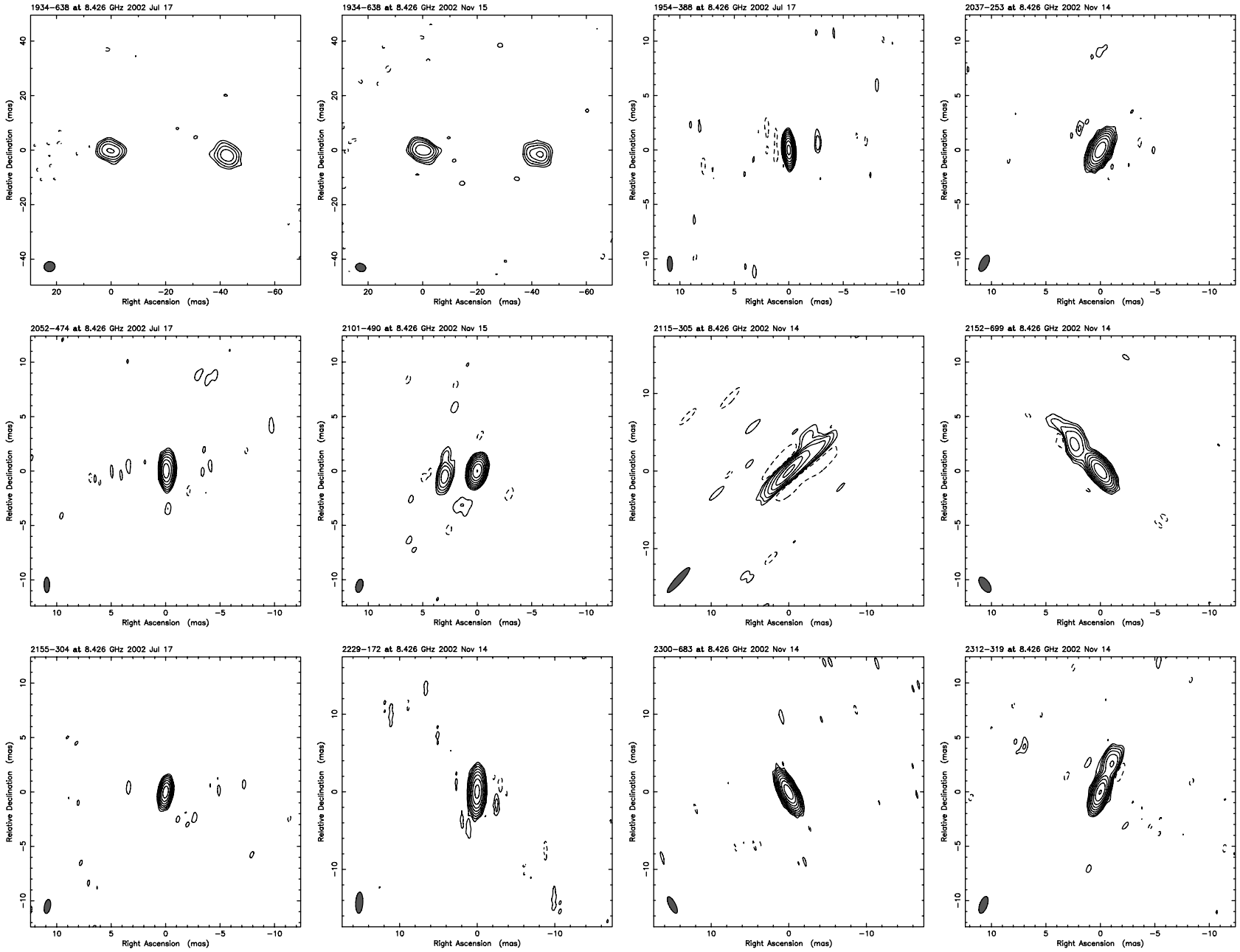

FIG. 1.—*Continued*

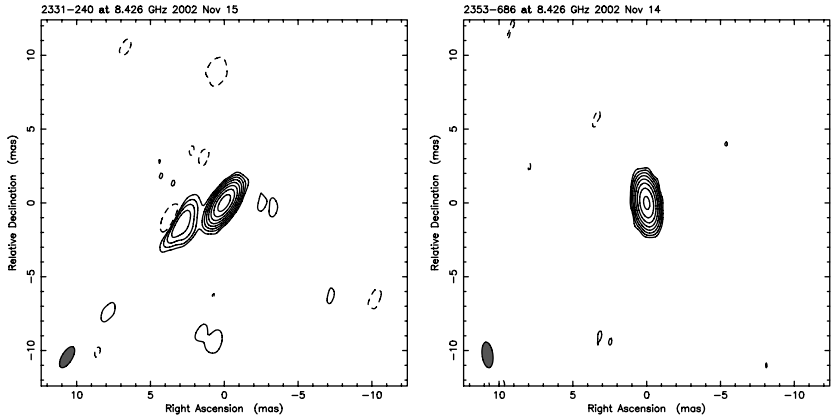

FIG. 1.—*Continued*

TABLE 2
PARAMETERS OF NATURALLY WEIGHTED IMAGES

SOURCE	BEAM[a]			PEAK	RMS[b]	CONTOUR LEVELS[c]
	a (mas)	b (mas)	ϕ (deg)	(Jy beam^{-1})	(mJy beam^{-1})	(mJy beam^{-1})
0008−264	1.6	0.7	−30	0.19	0.1	$0.4 \times (1, \ldots, 2^8)$
0118−272.....	1.5	0.7	−26	0.16	0.7	$2.0 \times (1, \ldots, 2^6)$
0130−171	1.6	0.9	−37	0.76	1.6	$4.9 \times (1, \ldots, 2^7)$
0131−522	2.0	0.5	10	0.46	0.3	$0.9 \times (1, \ldots, 2^9)$
0135−247	1.7	0.7	−28	0.24	0.2	$0.7 \times (1, \ldots, 2^8)$

NOTE.—Table 2 is presented in its entirety in the electronic version of the Astronomical Journal. A portion is shown here for guidance regarding its form and content.

[a] The restoring beam is an elliptical Gaussian with FWHM major axis a and minor axis b, with major axis in position angle ϕ (measured north through east).

[b] The root mean square of the residuals of the final hybrid image.

[c] Contours levels are represented by the geometric series $1, \ldots, 2^n$, e.g., for $n = 5$ the contour levels would be $\pm 1, 2, 4, 8, 16, 32$.

[d] Epoch 2002 July 16–20.

[e] Epoch 2002 November 14–16.

TABLE 3
PHYSICAL CHARACTERISTICS OF SOURCES

Source	Optical ID[a]	Redshift	Visual Magnitude
0008−264	Q	1.093	19.0
0118−272.....	L	>0.557[b]	15.6
0130−171	Q	1.020	18.44
0131−522	Q	0.020	20.0
0135−247	Q	0.831	17.3

NOTE.—Table 3 is presented in its entirety in the electronic version of the Astronomical Journal. A portion is shown here for guidance regarding its form and content.

[a] (Q) QSO; (G) galaxy; (L) BL Lacertae object; (A) other.

[b] Value given is a lower limit.

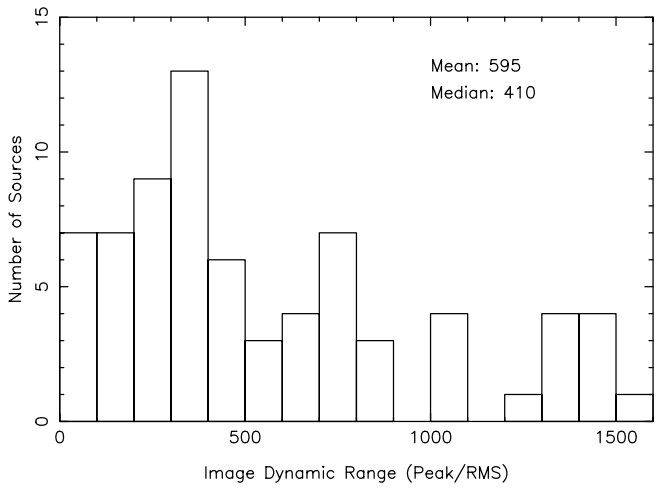

FIG. 2.—Distribution of image dynamic range for the 69 observed ICRF sources (five sources are imaged at two epochs and are counted twice in the distribution).

with a median of 410, indicating that most images have a useful dynamic range.

The LBA is an ad hoc array, and as such the location of the individual elements of the array is not optimal for generation of uniform *u-v* coverage. This relatively poor sampling in the *u-v* plane is the most important limitation on image quality. Representative plots of the *u-v* coverage for four sources at different declinations are shown in Figure 3. One important check on the robustness of our images is to compare the images of sources that are mutually visible to the VLBA and the LBA (PKS 0130−171, PKS 1143−245, PKS 1255−316, PKS 1424−418, PKS 1514−241, PKS 1519−273, PKS 1657−261, PKS 1908−201, PKS 1920−211, PKS 1954−388, PKS 2052−474, and PKS 2155−304). In every case, our images were consistent with those from the VLBA.[6] Another useful check is furnished by sources imaged at multiple epochs. All five sources for which we have images at two epochs, PKS 0332−403, PKS 1519−273, PKS 1622−297, PKS 1908−201, and PKS 1934−638, show consistent structures between those epochs (see Fig. 1). This suggests that our images are robust, reliable, and repeatable.

The distribution of source (VLBI) flux density is shown in Figure 4. Values range from a minimum of 40 mJy to a maximum of 2.8 Jy. The mean flux density is 0.72 Jy with a median of 0.54 Jy. With our 8 MHz bandwidth and 3 minute fringe-fit interval, the sensitivity for our most sensitive baseline, Parkes to the phased Australia Telescope Compact Array (ATCA, five of six dishes), is 0.32 mJy.

Gaussian models were fitted to the self-calibrated *visibility data* using the Caltech Difmap package. The results of the model fitting are listed in Table 4. After the source name, the following items are listed: component number, total component flux, distance of component from core, orientation of component with respect to the core component, length of major axis of component, axial ratio of component (1 for circular component), and orientation of major axis of component.

By inspection of the images and these fitted models, we can loosely classify the morphology of the sources into three groups. Thirty-two sources exhibit a compact structure with a single fitted component. The majority of the remaining sources (33) exhibit complex, multiple-component structure with well-separated components. Four sources show marginally resolved multiple-component structure.

It is generally believed that VLBI astrometric observations are most sensitive to the peak brightness in a source, as is evidenced by the change in astrometric position of 0923+392 (Fey, Eubanks, & Kingham 1997). Further, Fey & Charlot (1997, 2000) found correlations between the observed radio structure and the astrometric position accuracy and stability of the ICRF sources that they studied. These correlations indicate that the more extended sources have larger position uncertainties and are less positionally stable than the more compact sources. As an estimate of the compactness of the sources, we calculate the ratio of core flux density to total flux density. Core flux density is defined as the CLEANed flux density within one synthesized beam. The total flux density is defined as the total CLEANed flux density (i.e., the sum of all CLEAN components). The distribution of source compactness (ratio of core flux density to total flux density) is shown in Figure 5. Note that because of the inclusion of negative clean components, the source compactness can be greater than 1, as is the case for four sources included in this figure. With a mean value of 0.83 and a median of 0.88, Figure 5 indicates that most sources are relatively compact. Thus, inclusion of flux density information in the analysis suggests that many of the observed sources may be more suitable for reference-frame use than indicated by the above simple morphological classification. A more detailed analysis to determine the effects of the observed structure of these sources on their measured astrometric group delay (similar to the analysis of Fey & Charlot 1997, 2000) is the subject of future work and will be reported elsewhere.

4. SUMMARY

Imaging observations of 69 southern hemisphere ICRF sources are presented. Observations of the additional southern hemisphere ICRF sources will be reported as they are reduced and analyzed. We expect to be able to observe all sources at least twice and perhaps three times over the life of this project. This should allow us to produce time-dependent source models and evaluate the intrinsic structure and variability of the observed sources and their effect on astrometric position determination, thereby sustaining the viability of the ICRF.

Of the 69 sources presented in this paper, just under half show a single compact component. These should be well suited for reference-frame use. The remainder show extended structure in the form of multiple compact components but have most of their flux in a central component. These sources are less well suited for high-accuracy reference-frame use unless intrinsic structure can be taken into account. A more detailed analysis of the suitability of these sources for continued reference-frame use remains the subject of future work.

The imaging results presented here represent the most extensive VLBI survey of southern hemisphere extragalactic sources to date and, as such, provide a valuable tool for the investigation of a wide range of physical phenomena associated with these objects.

The hard work of the support and observing staff at all participating stations, as well as the ATNF correlator, is gratefully acknowledged. This research has made use of the US Naval Observatory (USNO) Radio Reference Frame Image Database. R. O. dedicates this paper to R. M. Deaker.

[6] The VLBA images can be found in the USNO Radio Reference Frame Image Database, at http://www.usno.navy.mil/RRFID/.

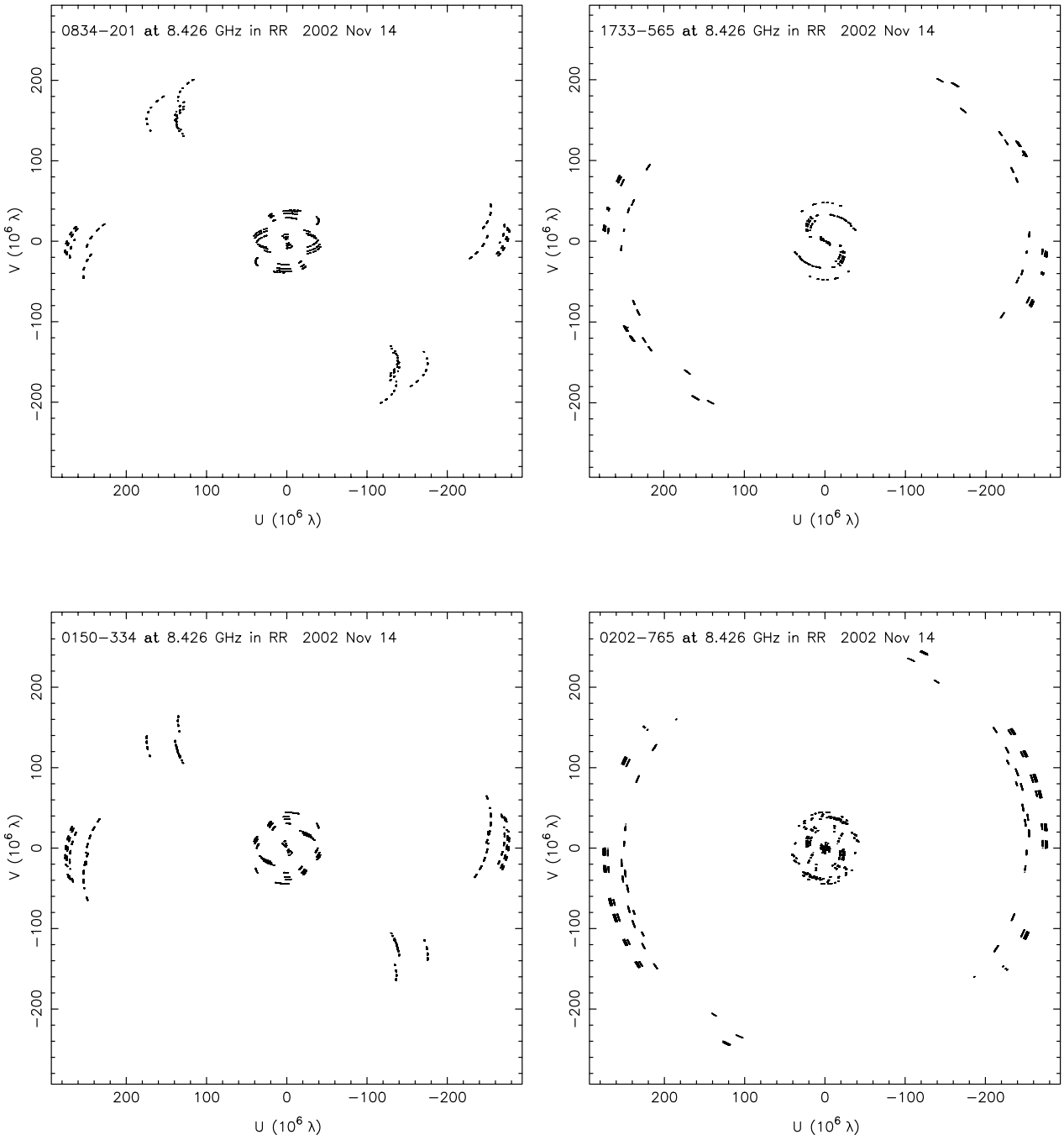

FIG. 3.—The *u-v* plane coverage of four sources at different declinations. The short baselines are generated by the "inner array" of Australian telescopes. The long-baseline tracks are added by Kokee and Hartebeesthoek. The "hole" in the *u-v* plane coverage results from the absence of telescopes between Australia and Hawaii/Hartebeesthoek.

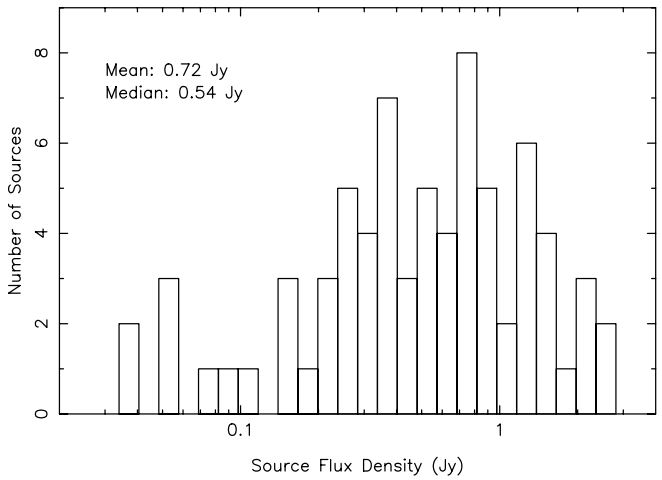

FIG. 4.—Distribution of source flux density for the 69 observed ICRF sources (five sources are imaged at two epochs and are counted twice in the distribution). Total flux density is defined as the total CLEANed flux density (i.e., the sum of all CLEAN components).

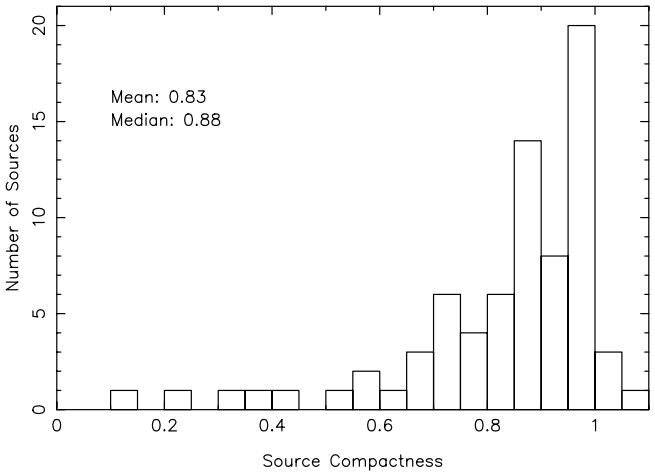

FIG. 5.—Distribution of source compactness (ratio of core flux density to total flux density) for the 69 observed ICRF sources (five sources are imaged at two epochs and are counted twice in the distribution). Core flux density is defined as the CLEANed flux density within one synthesized beam. The total flux density is defined as the total CLEANed flux density (i.e., the sum of all CLEAN components).

TABLE 4

GAUSSIAN MODELS

Source	Comp. No.	S (Jy)	r (mas)	θ (deg)	a (mas)	b/a	ϕ (deg)
0008−264	1	0.200	0.0	...	0.20	1.00	...
0118−272.....	1	0.178	0.0	...	0.37	0.62	−57
	2	0.153	10.3	−24	1.13	1.00	...
	3	0.014	4.0	−23	0.21	1.00	...
0130−171	1	0.833	0.0	...	0.35	0.00	57
0131−522	1	0.526	0.0	...	0.32	0.43	−68
	2	0.010	5.4	−169	0.43	1.00	...
0135−247	1	0.275	0.0	...	0.40	1.00	...
	2	0.042	2.4	74	1.08	1.00	...

NOTES.—The models fitted to the visibility data are of Gaussian form with flux density S and FWHM major axis a and minor axis b, with major axis in position angle ϕ (measured north through east). Components are separated from the (arbitrary) origin of the image by an amount r in position angle θ, which is the position angle (measured north through east) of a line joining the components with the origin. Table 4 is presented in its entirety in the electronic version of the Astronomical Journal. A portion is shown here for guidance regarding its form and content.

[a] Epoch 2002 July 16–20.

[b] Epoch 2002 November 14–16.

REFERENCES

Bridle, A. H., & Greisen, E. W. 1994, The NRAO AIPS Project: A Summary (AIPS Memo 87) (Socorro: NRAO)
Cannon, W. H., et al. 1997, Vistas Astron., 41, 297
Charlot, P. 1990, AJ, 99, 1309
Fey, A. L., & Charlot, P. 1997, ApJS, 111, 95
———. 2000, ApJS, 128, 17
Fey, A. L., Clegg, A. W., & Fomalont, E. B. 1996, ApJS, 105, 299
Fey, A. L., Eubanks, T. M., & Kingham, K. A. 1997, AJ, 114, 2284
Fey, A. L., et al. 2004a, AJ, 127, 3587
———. 2004b, AJ, 127, 1791
Greisen, E. W. 1988, The Astronomical Image Processing System (AIPS Memo 61) (Socorro: NRAO)
Johnston, K. J., et al. 1995, AJ, 110, 880
Johnston, K. J., Russell, J., de Vegt, C., Hughes, J., Jauncey, D., White, G., & Nicolson, G. 1988, in IAU Symp. 129, The Impact of VLBI on Astrophysics and Geophysics, ed. M. J. Reid & J. M. Moran (Dordrecht: Kluwer), 317
Kovalevsky, J., et al. 1997, A&A, 323, 620
Ma, C., et al. 1998, AJ, 116, 516
Ma, C., Shaffer, D. B., de Vegt, C., Johnston, K. J., & Russell, J. L. 1990, AJ, 99, 1284
Ojha, R., Fey, A. L., Johnston, K. J., Jauncey, D. L., Tzioumis, A. K., & Reynolds, J. E. 2004, AJ, 127, 1977
Pearson, T. J., & Readhead, A. C. S. 1984, ARA&A, 22, 97
———. 1988, ApJ, 328, 114
Perryman, M. A. C., et al. 1997, A&A, 323, L49
Preston, R. A., et al. 1989, AJ, 98, 1
Reynolds, J. E., Jauncey, D. L., Russell, J. L., King, E. A., McCulloch, P. M., Fey, A. L., & Johnston, K. J. 1994, AJ, 108, 725
Russell, J. L., et al. 1994, AJ, 107, 379
Shen, Z.-Q., et al. 1997, AJ, 114, 1999
———. 1998, AJ, 115, 1357
Shepherd, M. C. 1997, in ASP Conf. Ser. 125, Astronomical Data Analysis Software and Systems VI, ed. G. Hunt & H. E. Payne (San Francisco: ASP), 77
Taylor, G. B., Vermeulen, R. C., Readhead, A. C. S., Pearson, T. J., Henstock, D. R., & Wilkinson, P. N. 1996, ApJS, 107, 37
Wilson, W. E., Roberts, P. P., & Davis, E. R. 1996, in Proc. 4th Asia-Pacific Telescope Workshop, ed. E. A. King (Epping: Australia Telesc. Natl. Facility), 16